Polyyne formation *via* skeletal rearrangement induced by atomic manipulation

Niko Pavliček[1], Przemyslaw Gawel[2]*, Daniel R. Kohn[2], Zsolt Majzik[1], Yaoyao Xiong[2], Gerhard Meyer[1], Harry L. Anderson[2]* and Leo Gross[1]*

1 IBM Research—Zurich, Säumerstrasse 4, 8803 Rüschlikon, Switzerland

2 Department of Chemistry, Oxford University, Chemistry Research Laboratory, Oxford, OX1 3TA, United Kingdom

*email: lgr@zurich.ibm.com; przemyslaw.gawel@chem.ox.ac.uk; harry.anderson@chem.ox.ac.uk

Rearrangements that change the connectivity of a carbon skeleton are often useful in synthesis, but it can be difficult to follow their mechanisms. Scanning probe microscopy can be used to manipulate a skeletal rearrangement at the single-molecule level, while monitoring the geometry of reactants, intermediates and final products with atomic resolution. We studied the reductive rearrangement of 1,1-dibromo alkenes to polyynes on a NaCl surface at 5 K, a reaction that resembles the Fritsch-Buttenberg-Wiechell (FBW) rearrangement. Voltage pulses were used to cleave one C-Br bond, forming a radical, then to cleave the remaining C$^{\bullet}$-Br bond triggering the rearrangement. These experiments provide structural insight into the bromo-vinyl radical intermediates, showing that the C=C$^{\bullet}$–Br unit is nonlinear. Long polyynes, up to the octayne Ph-(C≡C)$_8$-Ph, have been prepared in this way. The control of skeletal rearrangements opens a new window on carbon-rich materials and extends the toolbox for molecular synthesis by atom manipulation.

Polyynes are widely investigated as precursors to functional materials[1], as molecular wires for charge transport[2] and because of their nonlinear optical properties[3]. They are also interesting models for carbyne, the elusive one-dimensional *sp*-hybridized allotrope of carbon[4,5]. Polyynes become increasingly unstable as the number of consecutive *sp*-carbon atoms is increased, due to their tendency to undergo cycloaddition and cross-linking reactions[6]. This problem can be alleviated by the presence of bulky terminal groups[3-5,7], and by supramolecular encapsulation[8,9]. The work presented here was initiated with the aim of fabricating and investigating long linear and cyclic polyynes[4,10] under highly controlled conditions on an inert surface.

The FBW rearrangement (Fig. 1)[11-14] has been known since 1894 and it is a widely used method for acetylene synthesis, particularly as the second step of the Corey-Fuchs reaction[15]. Tykwinski and coworkers were the first to report the migration of alkyne groups in a FBW rearrangement[16], and this has become a popular route for the synthesis of polyynes[7,14,17]. Early FBW rearrangements were carried out by deprotonation of a vinyl halide **1a**[18-20], but most modern examples use a 1,1-dihaloolefin **1b** as the starting material[14]. The 1,1-dihaloolefin is typically treated with butyl lithium to generate a carbenoid intermediate **2** (M = Li) *via* lithium-halogen exchange, but other reducing agents can be used, including samarium(II) iodide[21] and lanthanum metal[22]. Despite many investigations, the mechanism of the FBW rearrangement remains unclear. In some cases, there is evidence for formation of a carbene intermediate, **3**, which rearranges to the alkyne **4**, whereas in other cases the stereospecificity of the reaction demonstrates that the carbenoid **2** rearranges directly to the alkyne[18-20]. The reaction studied here is similar to a FBW rearrangement, in that it involves the reductive rearrangement of a 1,1-dibromoolefin to an alkyne, but it is different in that it occurs on a surface, reduction being achieved by electrons from the probe tip, whereas FBW rearrangements of 1,1-dibromoolefins are carried out in solution, typically using butyl lithium as the reducing agent.

Figure 1

Scanning probe microscopies, such as scanning tunneling microscopy (STM) and atomic force microscopy (AFM), were initially developed for imaging surfaces[23]. Atomic manipulation developed from the ability to place individual atoms on a surface using STM[24]. The resolution of molecular imaging was increased substantially by using AFM with CO-functionalized tips[25], which led to detailed characterization of a wide variety of molecular structures and thermally induced reactions on surface[26-35]. Atomic manipulation was extended towards triggering chemical reactions and single molecule synthesis[36]. Thermally induced on-surface synthesis is usually performed on catalytically active metal surfaces, whereas synthesis by atom manipulation can also be applied to molecules on thin insulating films such as NaCl. The inert NaCl surface and low temperature environment render it possible to stabilize and study reactive intermediates, such as arynes created by atom manipulation[37-40]. Furthermore, because of the decoupling by the insulating film, molecules can be characterized electronically using orbital imaging[41]. We set out to investigate an on-surface analogue of the FBW rearrangement, so as to learn about the mechanism and scope

of this reaction for preparing long polyynes under controlled conditions. In this work, we have generated tri-, tetra-, hexa- and octaynes (**5**–**8**) by atomic manipulation on bilayer NaCl islands on Cu(111) (Fig. 2). The tip of a low temperature qPlus-based[42] STM/AFM was used to cleave the C-Br bonds of precursors **5(Br2)**, **6(Br4)**, **7(Br4)**, and **8(Br4)** one-by-one using appropriate voltage pulses[37-39,43]. We have resolved the structures of molecular reactants, intermediates and products by AFM with CO-functionalized tips, providing a unique opportunity to investigate the geometries of these species and revealing the details of this intramolecular migration.

Figure 2

Results and discussion

Initially, we explored the generation of triyne **5** from precursor **5(Br2)** (Fig. 2a and Fig. 3). The structure of the dibromoolefin **5(Br2)** can be clearly distinguished from its AFM image (Fig. 3a). The triple bonds[27,32] and the attached Br atoms[38,43] can be assigned by their pronounced and characteristic contrast. A voltage pulse at $V \geq 1.7$ V was used to cleave the first C-Br bond. The AFM image of the resulting radical **5(Br)$^{\bullet}$** (Fig. 3b) shows a greater adsorption height of the phenyl ring adjacent to the remaining attached Br, resulting in a difference in contrast between the two phenyl rings. The detached Br atom remains nearby, but can be moved out of the frame by vertical manipulation[37,43]. A higher voltage pulse ($V \geq$ 2.1 V) was used to cleave the second C-Br bond resulting directly in formation of the triyne **5**.

Importantly, the NaCl bilayer is chemically inert which prevents reaction of radical intermediates with the surface[37-40]. The course of the reaction is very different when **5(Br2)** is manipulated on a bare Cu(111) surface; here a carbene is generated after the second debromination. This carbene seems to be bound to the Cu(111) surface and we never observed rearrangement under these conditions (see Supplementary Fig. 27). Similarly, on-surface annealing of a 1,1-dibromo alkene (**1b** with X = Br, R_1 = H and R_2 = biphenyl) on Au(111) monitored by STM/AFM imaging yields a cumulene without any rearrangement, as reported recently[35]. When the stepwise debromination was performed on several hundred individual **5(Br2)** molecules on Cu(111), statistical analysis showed that the voltage threshold of the first debromination is about 0.3 V smaller than for the second

debromination. We found single-electron processes with electron yields of about 10^{-9} for both the first debromination at V = 2.5 V and the second debromination at V = 2.8 V, respectively (see Supplementary Fig. 29). The tip position for the current injection is not critical, and the voltage pulse can be applied anywhere above the molecule on Cu(111) to induce the reactions. On bilayer NaCl, it is even possible to induce reactions nonlocally[44,45], i.e., by voltage pulses above the bare NaCl/Cu(111) substrate near the molecule, indicating mediation by NaCl/Cu(111) interface state electrons. Moreover, on bilayer NaCl both debromination reactions occur at lower absolute values of the voltage compared to Cu(111), which is tentatively explained by resonant tunneling into the LUMO facilitating vibrational excitations within the molecule[39].

Figure 3

Three intermediates were observed and characterized during formation of hexayne **7** from **7(Br4)** on NaCl. The AFM image of **7(Br4)** (see Fig. 4a) agrees well with its X-ray crystal structure (Supplementary Fig. 5); the triple bonds and the Br atoms have the expected characteristic contrast, similar to **5(Br2)**. Two consecutive voltage pulses at $V \geq 1.4$ V were applied to remove one of the two Br atoms at each olefin unit. The corresponding radical **7(Br3)$^{\bullet}$** and diradical **7(Br2)$^{2\bullet}$** were observed (Fig. 4b and Fig. 4c, respectively). We found that these radicals are always formed as the isomer with the bromine atoms pointing towards the center of the molecule. We never observed any intermediates in which two bromine atoms had been removed from one carbon atom leaving the other dibromoolefin unit intact, which is explained by the increased activation energy for the second debromination of an olefin unit. Next, a higher voltage pulse ($V \geq 2.0$ V) was applied to cleave the third C-Br bond, leading immediately to a 1,2-shift to form a tetrayne moiety on the left-hand side of the molecule (Fig. 4d). Finally, a fourth voltage pulse ($V \geq 2.0$ V) produced hexayne **7** (Fig. 4e). Generation of tetrayne **6** (Supplementary Fig. 24) and octayne **8** (Supplementary Fig. 26) proceeded similarly to the formation of **7**. Generally, adsorption on a planar surface tends to lead to a planar geometry of the molecules. Here, the phenyl groups are often tilted out of the surface plane by a small angle (on the order of few degrees[46]). The parts of the phenyl that appear brighter in the constant height AFM images feature a slightly increased adsorption height (cf. Figs. 3c and 4e)[46]. Beyond that, dibromoolefins **5(Br2)**, **7(Br4)**, and **8(Br4)** are relatively flat, both on the surface and in the solid state (see crystal structures in the Supplementary Section 3). In contrast, the two

phenyl rings of **6(Br4)** are twisted out of the plane of the dibromoolefin (by 70° in the solid state [Supplementary Fig. 3] and 52° in vacuum according to calculations [Supplementary Fig. 11]), which accounts for the low resolution of AFM images of **6(Br4)** (Supplementary Fig. 24).

Figure 4

The higher voltage required to break the C-Br bonds in the vinyl C=C$^{\bullet}$-Br radicals (Br dissociation form **5(Br)$^{\bullet}$**, **7(Br2)$^{2\bullet}$** and **7(Br)$^{\bullet}$**), compared to dissociation of Br from C=CBr$_2$ (Br dissociation from **5(Br2)**, **7(Br4)** and **7(Br3)$^{\bullet}$**), indicates that cleavage of the second C-Br bond in the vinyl radical is the rate determining step of the rearrangement. We never observe a carbene intermediate (**3** in Fig. 1) on NaCl during these reactions under our experimental conditions. The 1,2-bond migration in our manipulation experiments always takes place after cleavage of the second C-Br bond of a dibromoolefin unit; we conclude that the activation energy for the 1,2-shift is lower than that for removal of the second bromine atom. Although the time resolution of our AFM experiments is on the order of a few minutes, a carbene intermediate with a barrier to thermally activated 1,2-shift greater than 15 meV would be observable on this timescale at T = 5 K. Quantum chemical calculations indicate that the barrier to the 1,2-shift of this type of carbene in the gas phase is about 200 meV (see Supplementary Fig. 22)[47], indicating that the reaction on NaCl does not involve the thermally activated rearrangement of a carbene, or that the energy barrier is significantly lowered by the surface.

There has been some discussion about the bond angles in vinyl radicals of the type R$_2$C=C$^{\bullet}$-X because these species can be linear or bent, depending on the substituents R and X (Ref 48). The high resolution of images of **5(Br)$^{\bullet}$**, **7(Br2)$^{2\bullet}$**, and **7(Br)$^{\bullet}$** show that the C=C$^{\bullet}$-Br radical is nonlinear. This is the first time that the geometry of a vinyl radical has been visualized and the result is in good agreement with DFT calculations, which predict an angle of 133° in **5(Br)$^{\bullet}$** (Supplementary Fig. 10). The geometry that we observe in these radicals agrees with the angle in H$_2$C=C$^{\bullet}$-Br radicals deduced from IR spectroscopy and computational studies[49].

Polyynes **5**–**8** were characterized by AFM, STM, and scanning tunneling spectroscopy (STS, Fig. 5). Some of the images of these polyynes show a curved geometry, as often observed for longer polyynes[5]. In general, for a neutral molecule, the LUMO or HOMO

densities are probed by applying a positive or negative sample voltage large enough to attach or detach an electron to or from the molecule, respectively. Images at these voltages, corresponding to tunneling *via* the negative or positive ion resonance (NIR or PIR) reflect the densities of LUMO or HOMO, respectively[41]. We recorded images of the NIR (corresponding to the density of the LUMO) of polyynes **5**–**8**. It is possible to see the characteristic nodes in the middle of every triple bond in the images of **7** and **8** recorded with functionalized tips (Figs. 5e and 5k), in agreement with DFT-calculated LUMOs (Figs. 5f and 5l). We also recorded images for the PIR (HOMO) of **7** and **8** (Figs. 5b and 5h). The differential conductance spectra show that the LUMO energies of the polyynes decrease for longer polyynes as expected (Fig. 5m). We have compared the experimentally determined resonance energies (see Supplementary Fig. 30), to theoretically calculated electronic HOMO-LUMO gaps (Fig. 5n). It is known, that Kohn-Sham DFT tends to underestimate the electronic gap. We have used many-body perturbation theory in the *GW* approximation, accounting for the screened Coulomb interaction *W* related to temporary charging using a Green's function approach, to obtain more accurate quasiparticle energies[28,40]. We obtained good agreement between experimental STS data and theoretical *GW* quasiparticle levels, shown in Fig. 5n.

Figure 5

Conclusions

We have synthesized a series of polyynes **5**–**8** using atomic manipulation on bilayer NaCl on Cu(111), starting from the corresponding dibromoolefins, while characterizing the intermediates, and all the final polyynes using AFM, STM, and STS. The core transformation in this approach is a 1,2-shift similar to the FBW rearrangement, initiated by the dissociation of the Br from the vinyl radical (C=C$^{\bullet}$-Br). This is the first report of any 1,2-shift triggered by atomic manipulation on a surface. In the case of **5** and **7**, we were able to image all of the vinyl radical intermediates, and these radicals were found to be persistent on the surface at 5 K. We do not observe any carbene intermediates on NaCl and conclude that the activation energy for the 1,2-shift is lower than that for the cleavage of the C$^{\bullet}$-Br bond. In contrast, on Cu we observed the carbene bonded to the surface and the rearrangement does not occur.

We have demonstrated that complex molecular skeletal rearrangements can be triggered

by atom manipulation. This is the first time that polyynes have been structurally characterized by STM and AFM. The precision of the synthesis and wealth of information provided by this approach opens new opportunities for the on-surface fabrication of novel molecules and atomic scale devices.

Methods

Synthesis

Compounds **5(Br2)**, **7(Br4)** and **8(Br4)** were prepared using published procedures, as summarized in the Supplementary Information; all characterization data match those previously reported. The synthesis and characterization of the compound **6(Br4)** and additional details of synthetic methods and characterization are available in the Supplementary Information.

Microscopy

The experiments were carried out in homebuilt combined STM and AFM systems operated under ultrahigh vacuum conditions (base pressure $p < 10^{-10}$ mbar) at a temperature of $T = 5$ K. The microscopes were equipped with qPlus sensors[42] operated in frequency-modulation mode[50]. Two sensors were used with eigenfrequencies of $f_0 \approx 28.8$ kHz and $f_0 \approx 30.1$ kHz, respectively, a stiffness of $k = 1800$ N/m and quality factors of $Q = 20{,}000$ and $Q = 150{,}000$, respectively. The oscillation amplitude was set to $A = 50$ pm, and the voltage V was applied to the sample.

STM images recorded in constant-current (closed feedback loop) and constant-height (open feedback loop) mode show the topography z and the tunneling current I, respectively. STM images were acquired using different tip functionalizations (Cu tip, CO tip, Br tip)[43] as indicated in each STM image. AFM images were acquired with a CO-terminated tip in constant-height mode (open feedback loop) and show the frequency shift Δf. The tip-height offset is given for each AFM image with respect to a STM set point of 1 pA at 0.1 V above the bare surface (Cu or NaCl). Positive height offsets refer to a distance increase.

A Cu(111) single crystal was cleaned by sputtering and annealing cycles. Experiments were performed on the bare Cu(111) surface, and on islands of two-monolayer thick NaCl. NaCl islands were grown by sublimation from a crucible onto the cleaned Cu(111) surface held at a temperature of 270 K. Low sub-monolayer coverages of compounds **5(Br2)**, **6(Br4)**, **7(Br4)**, **8(Br4)**, and CO molecules were deposited at sample temperatures $T < 10$ K.

STM and AFM images, as well as numerically obtained dI/dV (V) curves, were post-processed using Gaussian low-pass filters.

Data availability

The crystallographic data have been deposited (CCDC 1567546 (**7(Br4)**), 1567547 (**6(Br4)**), 1567548 (**8(Br4)**)), and copies of these data can be obtained free of charge from the Cambridge Crystallographic Data Centre, 12 Union Road, Cambridge CB2 1EZ, UK (fax: +44(1223)-336-033; e-mail: deposit@ccdc.cam.ac.uk), or *via* www.ccdc.cam.ac.uk/data_request/cif. Corresponding .cif files including X-ray crystal

structures and .xyz files containing geometries of calculated structures are available as Supplementary Information of this manuscript. The other data that support the findings of this study are available from the corresponding authors upon reasonable request.

Acknowledgement

The research leading to these results received funding from the ERC Advanced Grants CEMAS (agreement no. 291194) and CoSuN (320969), the ERC Consolidator Grant AMSEL (682144), and the EU project PAMS (610446). P.G. acknowledges the receipt of Postdoc.Mobility fellowships from the Swiss National Science Foundation. Y.X. was supported by the EPSRC Centre for Doctoral Training in Synthesis for Biology and Medicine (EP/L015838/1) and by a University of Oxford Clarendon Fund Scholarship. The authors would like to acknowledge the use of the Oxford Advanced Research Computing (ARC) facility in carrying out the computational work. DOI: 10.5281/zenodo.22558. We thank Prof. Robert S. Paton and Isabell Gruebner for discussions on computational studies and Dr. Amber L. Thompson for help with X-ray crystal structure refinements.

Author contributions

P.G. conceived the project. N.P., Z.M., G.M. and L.G. performed the STM/AFM experiments and analysis. P.G. and D.R.K. performed the organic synthesis. Y.X. measured and solved X-ray crystal structures. H.L.A. contributed to the design of the study. All the authors analyzed the results and contributed to the manuscript.

Competing financial interests

The authors declare no competing financial interests.

References

1. Schrettl, S., *et al*. Functional carbon nanosheets prepared from hexayne amphiphile monolayers at room temperature. *Nat. Chem.* **6**, 468–476 (2014)
2. Wang, C., *et al.* Oligoyne single molecule wires. *J. Am. Chem. Soc.* **131**, 15647–15654 (2009).
3. Eisler, S., *et al*. Polyynes as a model for carbyne: synthesis, physical properties, and nonlinear optical response. *J. Am. Chem. Soc.* **127**, 2666–2676 (2005).
4. Diederich, F. Carbon scaffolding: building acetylenic all-carbon and carbon-rich compounds. *Nature* **369**, 199–207 (1994).
5. Tykwinski, R. R. Carbyne: the molecular approach. *Chem. Rec.* **15**, 1060–1074 (2015).
6. Hoye, R. H., Baire, B., Niu, D., Willoughby, P. H. & Woods, B. P. The hexadehydro-Diels-Alder reaction. *Nature* **490**, 208–212 (2012).
7. Chalifoux, W. A. & Tykwinski, R. R. Synthesis of polyynes to model the *sp*-carbon allotrope carbyne. *Nat. Chem.* **2**, 967–971 (2010).
8. Stahl, J., *et al.* sp Carbon chains surrounded by sp^3 carbon double helices: a class of molecules that are accessible by self-assembly and models for “insulated” molecular-scale devices. *Angew. Chem. Int. Ed.* **41**, 1871–1876 (2002).

9. Movsisyan, L. D., *et al.* Polyyne rotaxanes: stabilization by encapsulation. *J. Am. Chem. Soc.* **138**, 1366–1376 (2016).
10. Diederich, F., *et al.* All-carbon molecules: evidence for the generation of cyclo[18]carbon from a stable organic precursor. *Science* **245**, 1088–1090 (1989).
11. Fritsch, P. IV. Ueber die Darstellung von Diphenylacetaldehyd und eine neue Synthese von Tolanderivaten. *Liebigs Ann. Chem.* **279**, 319–323 (1894).
12. Buttenberg, W. P. Condensation des Dichloracetals mit Phenol und Toluol. *Liebigs Ann. Chem.* **279**, 324–337 (1894).
13. Wiechell, H. Condensation des Dichloracetals mit Anisol und Phenetol. *Liebigs Ann. Chem.* **279**, 337–344 (1894).
14. Jahnke, E. & Tykwinski, R. R. The Fritsch-Buttenberg-Wiechell rearrangement: modern applications for an old reaction. *Chem. Commun.* **46**, 3235–3249 (2010).
15. Corey, E. J. & Fuchs, P. L. A synthetic method for formyl→ethynyl conversion (RCHO→RC≡CH or RC≡CR'). *Tetrahedron Lett.* **13**, 3769–3772 (1972).
16. Eisler, S. & Tykwinski, R. R. Migrating alkynes in vinylidene carbenoids: an unprecedented route to polyynes. *J. Am. Chem. Soc.* **122**, 10736–10737 (2000).
17. Luu, T., Morisaki, Y., Cunningham, N. & Tykwinski, R. R. One-pot formation and derivatization of di- and triynes based on the Fritsch−Buttenberg−Wiechell rearrangement. *J. Org. Chem.* **72**, 9622–9629 (2007).
18. Stang, P. J. Unsaturated carbenes. *Chem. Rev.* **78**, 383–405 (1978).
19. Knorr, R. Alkylidenecarbenes, alkylidenecarbenoids, and competing species: which is responsible for vinylic nucleophilic substitution, [1+2] cycloadditions, 1,5-CH insertions, and the Fritsch-Buttenberg-Wiechell rearrangement? *Chem. Rev.* **104**, 3795–3849 (2004).
20. Pritchard, J. G. & Bothner-By, A. A. Base-initiated dehydrohalogenation and rearrangement of 1-halo-2,2-diphenylethylenes in *t*-butyl alcohol. The effect of deuterated solvent. *J. Phys. Chem.* **64**, 1271–1277 (1960).
21. Kunishima, M., Hioki, K., Ohara, T. & Tani, S. Generation of alkylidenecarbenes from 1,1-dibromoalk-1-enes by the reaction with samarium diiodide in hexamethylphosphoric triamide-benzene. *J. Chem. Soc., Chem. Commun.* 219–220 (1992).
22. Umeda, R., Yuasa, T., Anahara, N. & Nishiyama Y. Fritsch-Buttenberg-Wiechell rearrangement to alkynes from *gem*-dihaloalkenes with lanthanum metal. *J. Organomet. Chem.* **696**, 1916–1919 (2011).
23. Binnig, G. & Rohrer, H. Scanning tunneling microscopy - from birth to adolescence. *Angew. Chem. Int. Ed. Engl.* **26**, 606–614 (1987).
24. Eigler, D. M., Schweizer, E. K. Positioning single atoms with a scanning tunnelling microscope. *Nature* **344**, 524–526 (1990).
25. Gross, L., Mohn, F., Moll, N., Liljeroth, P. & Meyer, G. The chemical structure of a molecule resolved by atomic force microscopy. *Science* **325**, 1110–1114 (2009).
26. Gross, L., *et al.* Organic structure determination using atomic-resolution scanning probe microscopy. *Nat. Chem.* **2**, 821–825 (2010).
27. de Oteyza, D. G. *et al.* Direct Imaging of Covalent Bond Structure in Single-Molecule Chemical Reactions. *Science* **340**, 1434–1437 (2013).
28. Ruffieux, P., *et al.* On-surface synthesis of graphene nanoribbons with zigzag edge topology. *Nature* **531**, 489–493 (2016).

29. He, Y. *et al.* Fusing tetrapyrroles to graphene edges by surface-assisted covalent coupling. *Nat. Chem.* **9**, 33–38 (2016).
30. Sun, Q., *et al.* Bottom-up synthesis of Metalated Carbyne. *J. Am. Chem. Soc*. **138**, 1106–1109 (2016).
31. Kawai, S. *et al.* Thermal control of sequential on-surface transformation of a hydrocarbon molecule on a copper surface, *Nat. Comm.* **7**, 12711 (2016).
32. Riss, A. *et al.* Imaging single-molecule reaction intermediates stabilized by surface dissipation and entropy. *Nat. Chem.* **8**, 678–683 (2016).
33. Stetsovych, O. *et al.* From helical to planar chirality by on-surface chemistry. *Nat. Chem.* **9**, 213–218 (2017).
34. Shiotari, A. *et al.* Strain-induced skeletal rearrangement of a polycyclic aromatic hydrocarbon on a copper surface. *Nat. Comm.* **8**, 16089 (2017).
35. Sun, Q. *et al.* On-surface formation of cumulene by dehalogenative homocoupling of alkenyl gem-dibromides. *Angew. Chem. Int. Ed.* **56**, 12165–12169 (2017).
36. Hla, S.-W., Bartels, L., Meyer, G. & Rieder, K.-H. Inducing All Steps of a Chemical Reaction with the Scanning Tunneling Microscope Tip: Towards Single Molecule Engineering. *Phys. Rev. Lett.* **85**, 2777–2780 (2000).
37. Pavliček, N. *et al.* On-surface generation and imaging of arynes by atomic force microscopy. *Nat. Chem.* **7**, 623–628 (2015).
38. Schuler, B. *et al.* Reversible Bergman cyclization by atomic manipulation. *Nat. Chem.* **8**, 220–224 (2016).
39. Pavliček, N., Majzik, Z., Collazos, S., Meyer, G., Pérez, D., Guitian, E., Peña, D. & Gross, L. Generation and Characterization of a *Meta*-Aryne on Cu and NaCl Surfaces. *ACS Nano*, **11**, 10768–10773 (2017).
40. Pavliček, N. *et al.* Synthesis and characterization of triangulene. *Nat. Nanotech.* **12**, 308–311 (2017).
41. Repp, J., Meyer, G., Stojković, S. M., Gourdon, A. & Joachim, C. Molecules on Insulating Films: Scanning-Tunneling Microscopy Imaging of Individual Molecular Orbitals. *Phys. Rev. Lett.* **94**, 026803 (2005).
42. Giessibl, F. J. High-speed force sensor for force microscopy and profilometry utilizing a quartz tuning fork. *Appl. Phys. Lett.* **73**, 3956–3958 (1998).
43. Mohn, F., Schuler, B., Gross, L. & Meyer, G. Different tips for high-resolution atomic force microscopy and scanning tunneling microscopy of single molecules. *Appl. Phys. Lett.* **102**, 073109 (2013).
44. Schendel, V., Borca, B., Pentegov, I., Michnowicz, T., Kraft, U., Klauk, H., Wahl, P., Schlickum, U. & Kern, K. Remotely Controlled Isomer Selective Molecular Switching. *Nano Lett.* **16**, 93–97 (2015).
45. Ladenthin, J. N., Grill, L., Gawinkowski, S., Liu, S., Waluk, J. & Kumagai, T. Hot Carrier-Induced Tautomerization within a Single Porphycene Molecule on Cu (111). *ACS Nano* **9**, 7287–7295 (2015).
46. Schuler, B. *et al.* Adsorption geometry determination of single molecules by atomic force microscopy. *Phys. Rev. Lett.* **111,** 106103 (2013).
47. Moore K. A., Vidaurri-Martinez J. S. & Thamattoor D. M. The Benzylidenecarbene–Phenylacetylene Rearrangement: An Experimental and Computational Study. *J. Am. Chem. Soc.* **134**, 20037–20040 (2012).

48. Galli, C., Guarnieri, A., Koch, H., Mencarelli, P. & Rappoport, Z. Effect of substituents on the structure of the vinyl radical: calculations and experiments. *J. Org. Chem.* **62**, 4072–4077 (1997).
49. Zhu, C., Duarte, L. & Khriachtchev, L. Matrix-isolation and computational study of H_2CCCl and H_2CCBr radicals. *J. Chem. Phys.* **145**, 074312 (2016).
50. Albrecht, T. R., Grütter, P., Horne, D. & Rugar, D. Frequency modulation detection using high-Q cantilevers for enhanced force microscope sensitivity. *J. Appl. Phys.* **69**, 668–673 (1991).

Figure 1. Fritsch-Buttenberg-Wiechell rearrangement. (X = halogen; M = electropositive metal; R^1, R^2 = aryl, alkyl, vinyl or alkynyl; **1a**: 1-haloolefin; **1b**: 1,1-dihaloolefin; **2**: carbenoid intermediate; **3**: carbene intermediate; **4**: alkyne). Reaction of **1a** requires a base whereas reaction of **1b** requires a reducing agent such as BuLi.

Figure 2. On-surface reactions studied in this work. Only one radical intermediate was observed during formation of **5** from **5(Br2)**, whereas during the formation of **7** from **7(Br4)** two radical intermediates were observed, as well as the diradical **7(Br2)$^{2\bullet}$** shown, due to the sequential loss of the four bromine atoms.

Figure 3. On-surface reaction to generate triyne **5** from precursor **5(Br2)** on bilayer NaCl on Cu(111). **a**, **b**, and **c** are constant-height, CO-tip AFM images of precursor **5(Br2)**, intermediate radical **5(Br)$^{\bullet}$** and triyne **5**, respectively. The two Br atoms have been successively dissociated by voltage pulses from the tip. The range of the grayscale representing the frequency shift Δf is indicated for each AFM image, and the tip-height offset Δz is given with respect to a STM set point of I = 1 pA at V = 0.1 V above the bare surface. **d–f**, Corresponding Laplace-filtered AFM images with structural ball-and-stick models overlaid as a visual aid. Grey, red, and white balls represent C, Br, and H, respectively.

Figure 4. On-surface reaction to generate hexayne 7 from precursor **7(Br4).** Panels **a–e** show AFM images of **a** precursor **7(Br4)**, **b** radical **7(Br3)$^{\bullet}$**, **c** diradical **7(Br2)$^{2\bullet}$**, **d** intermediate **7(Br)$^{\bullet}$** after the first 1,2-shift, resulting in a tetrayne moiety, and **e** hexayne **7** after second 1,2-shift. The tip-height offsets Δz with respect to a STM set point of I = 1 pA at V = 0.1 V above the bare surface are indicated. The four Br atoms have been successively dissociated by voltage pulses from the tip. **f–j**, Respective Laplace-filtered AFM images with structural ball-and-stick models overlaid as a visual aid. All panels show the evolution of the same molecule.

Figure 5. Characterization of polyynes **5–8** on NaCl using AFM, STM, and STS. Panels **a** and **g** show constant-height CO-tip AFM images, at the respective tip-height offsets Δz indicated, of hexayne **7** (repeated from Fig. 4e) and octayne **8** (anchored at a step edge of a three-monolayer thick NaCl island). Panels **b–f** and **h–l** show corresponding STM images of the PIR (const. height) and NIR (const. height and const. current) with different tip terminations as indicated at the sample voltages V, in comparison to DFT-calculated HOMO and LUMO densities, respectively. **m**, Typical differential conductance (dI/dV) spectra for polyynes **5–8** at setpoints of I = 1 pA at V = 2.3 V for **5**, 2.1 V for **6**, 1.5 V for **7** and 1.4 V for **8**, respectively, obtained above a terminal phenyl group as indicated by a cross in **a** and **g**. **n**, Transport gap as a function of triple bond units. Zero voltage of quasiparticle values corresponds to a work function of 4.0 eV for bilayer NaCl on Cu(111). Experimental values in colored, solid symbols; theoretical values calculated using the GW approximation in gray, open symbols; dashed lines, connecting the theoretical values are drawn as a guide to the eye. For every image the corresponding grayscale of the measured variable (frequency shift Δf, tunneling current I or tip height z) is indicated together with the range of the grayscale.

Figure 1

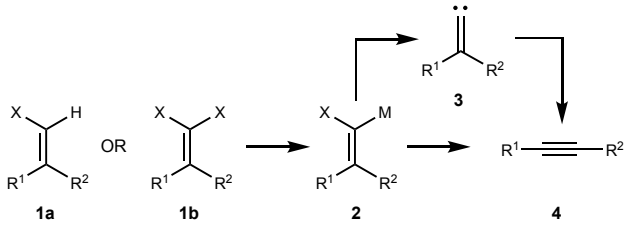

Figure 2

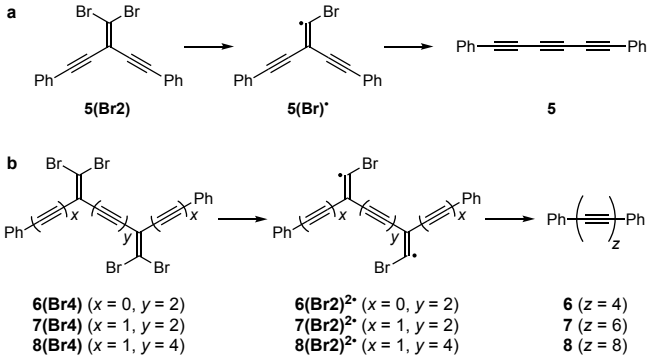

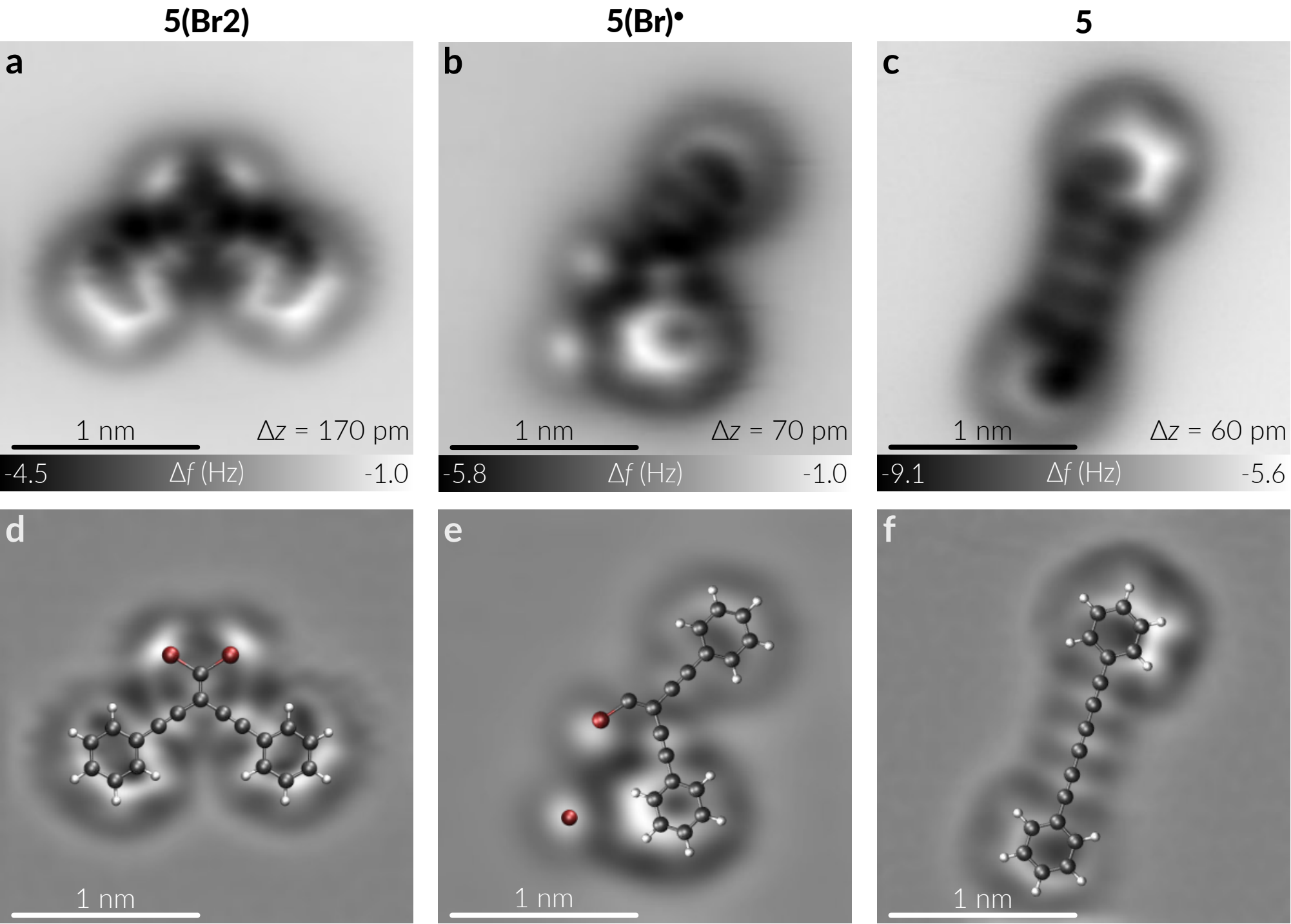
5(Br2)
5(Br)•
5
a
1 nm
Δz = 170 pm
-4.5
Δf (Hz)
-1.0
b
1 nm
Δz = 70 pm
-5.8
Δf (Hz)
-1.0
c
1 nm
Δz = 60 pm
-9.1
Δf (Hz)
-5.6
d
1 nm
e
1 nm
f
1 nm

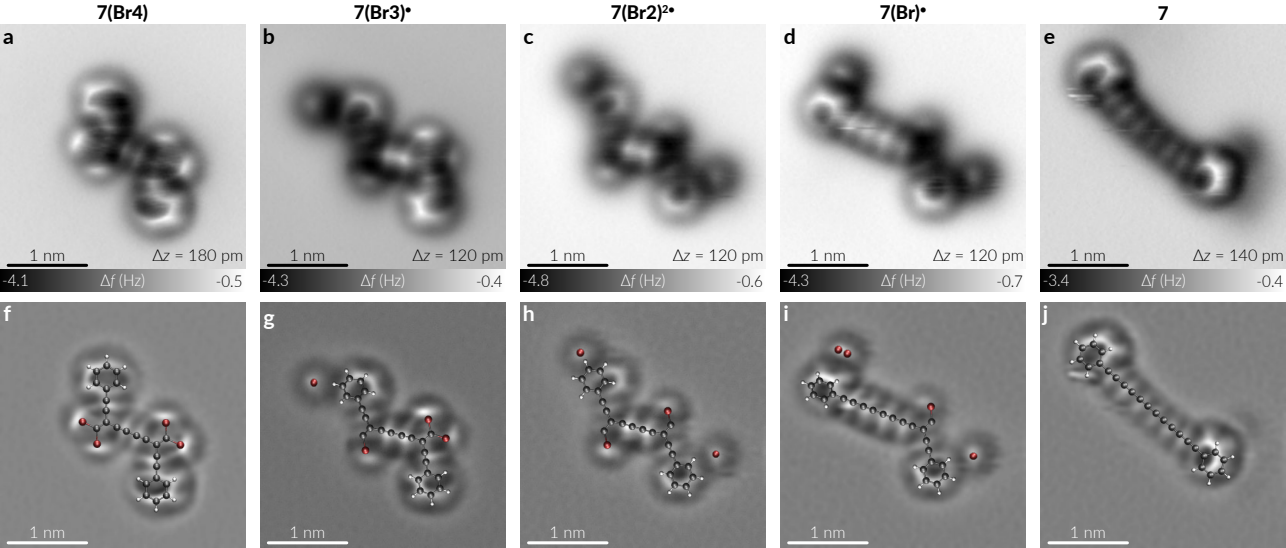
7(Br4)
7(Br3)•
7(Br2)2•
7(Br)•
7
a
b
c
d
e
1 nm
Δz = 180 pm
Δz = 120 pm
Δz = 120 pm
Δz = 120 pm
Δz = 140 pm
-4.1
Δf (Hz)
-0.5
-4.3
-0.4
-4.8
-0.6
-4.3
-0.7
-3.4
-0.4
f
g
h
i
j
1 nm

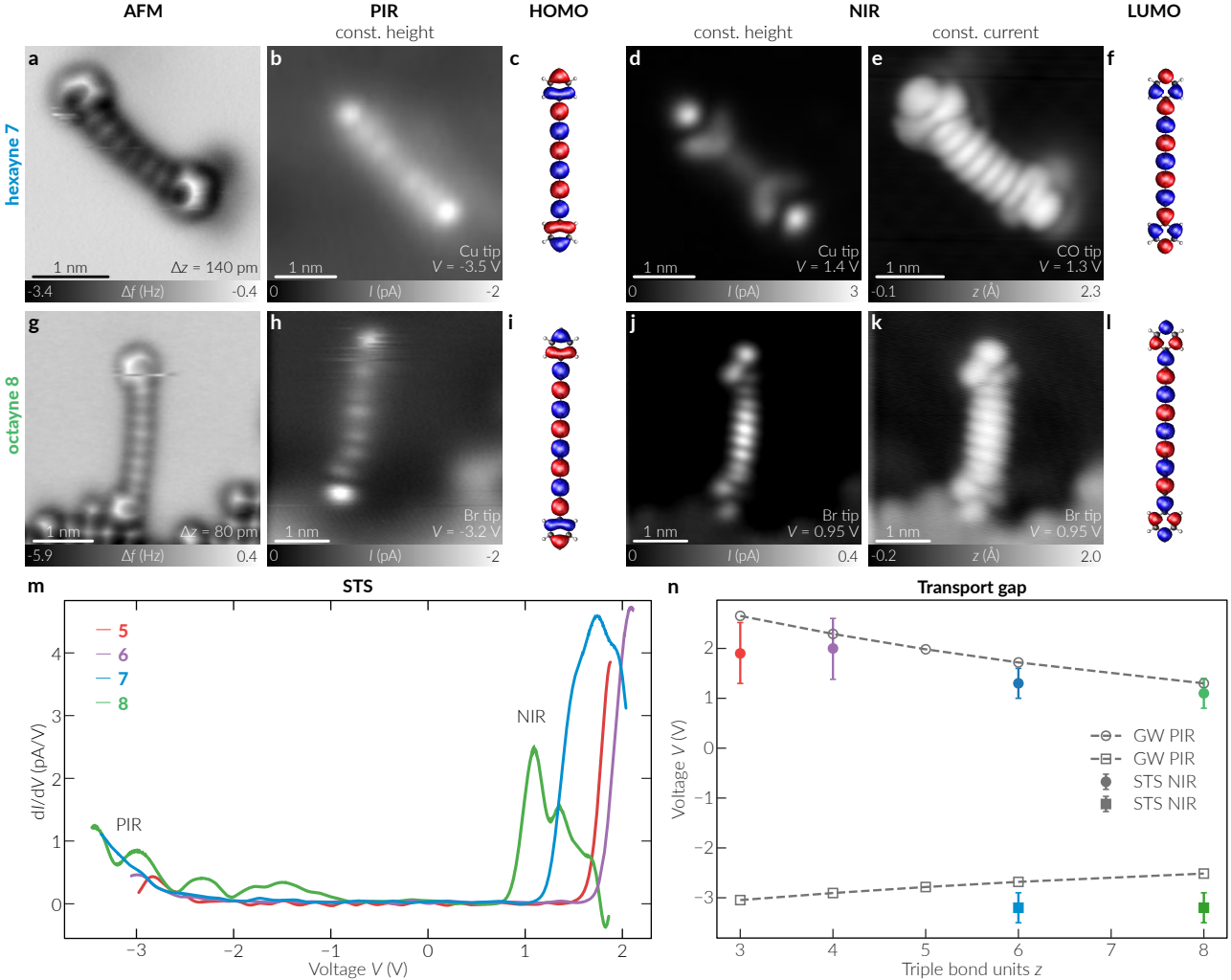
AFM
PIR
const. height
HOMO
NIR
const. height
const. current
LUMO
hexayne 7
octayne 8
a
b
c
d
e
f
g
h
i
j
k
l
1 nm
Δz = 140 pm
Cu tip
V = -3.5 V
Cu tip
V = 1.4 V
CO tip
V = 1.3 V
Δz = 80 pm
Br tip
V = -3.2 V
Br tip
V = 0.95 V
Br tip
V = 0.95 V
-3.4
Δf (Hz)
-0.4
0
I (pA)
-2
0
I (pA)
3
-0.1
z (Å)
2.3
-5.9
Δf (Hz)
0.4
0
I (pA)
-2
0
I (pA)
0.4
-0.2
z (Å)
2.0
m
STS
5
6
7
8
NIR
PIR
dI/dV (pA/V)
Voltage V (V)
n
Transport gap
GW PIR
GW PIR
STS NIR
STS NIR
Voltage V (V)
Triple bond units z